Lab on a Chip

PAPER

View Article Online
View Journal | View Issue

Cite this: *Lab Chip*, 2016, **16**, 1393

3D printed nervous system on a chip†

Blake N. Johnson,[ab] Karen Z. Lancaster,[c] Ian B. Hogue,[c] Fanben Meng,[bd] Yong Lin Kong,[b] Lynn W. Enquist[c] and Michael C. McAlpine*[bd]

Received 14th October 2015,
Accepted 8th December 2015

DOI: 10.1039/c5lc01270h

www.rsc.org/loc

Bioinspired organ-level *in vitro* platforms are emerging as effective technologies for fundamental research, drug discovery, and personalized healthcare. In particular, models for nervous system research are especially important, due to the complexity of neurological phenomena and challenges associated with developing targeted treatment of neurological disorders. Here we introduce an additive manufacturing-based approach in the form of a bioinspired, customizable 3D printed nervous system on a chip (3DNSC) for the study of viral infection in the nervous system. Micro-extrusion 3D printing strategies enabled the assembly of biomimetic scaffold components (microchannels and compartmented chambers) for the alignment of axonal networks and spatial organization of cellular components. Physiologically relevant studies of nervous system infection using the multiscale biomimetic device demonstrated the functionality of the *in vitro* platform. We found that Schwann cells participate in axon-to-cell viral spread but appear refractory to infection, exhibiting a multiplicity of infection (MOI) of 1.4 genomes per cell. These results suggest that 3D printing is a valuable approach for the prototyping of a customized model nervous system on a chip technology.

Introduction

The development of hierarchal organ-level platforms, known as organs-on-chips,[1–5] as potential complements and replacements for the extensive use of small animal models, has arisen as a critical area in fundamental and clinical research.[4] To date, organs-on-chips have been primarily developed *via* microfabrication, which has led to a number of impressive demonstrations.[1,3,6–8] Yet, this approach requires subsequent biofunctionalization and validation steps due to processing conditions which are not amenable to biological functionalities. It would be desirable to merge the capabilities of computer-driven material assembly, rapid prototyping, and controlled biofunctionalization in a one-pot manufacturing approach for *in vitro* systems.

3D printing has evolved as an enabling technology for the development of advanced materials and devices,[9–13] with applications in conformal electronics,[14–16] biomedical devices,[17–19] and prosthetics.[20,21] The scope of 3D printed materials is expanding, and already includes smart materials,[22] nanomaterials,[14,16,21] biomaterials,[21] living materials (*e.g.* cell-laden matrices),[23] and combinations of these for novel biotechnologies. For example, tissue constructs,[17,24–26] organs,[2,26,27] biosensors,[28,29] actuators,[30] and even bionic organs[21] have recently been fabricated. The palette of fundamental materials research and novel applications in the 3D printing space is rapidly evolving. Indeed, 3D printing may offer a potential solution for developing next-generation organ-on-a-chip technologies,[31] as it provides a bottom-up manufacturing paradigm for chip customization, rapid prototyping, and multimaterial processing capabilities.

Among the organ systems of interest – including the cardiovascular, digestive, endocrine, muscular, nervous, respiratory, and skeletal systems[6,32–34] – the development of *in vitro* models for the nervous system is vital, as the treatment of neurological disorders is a critical medical challenge. As a result, various microfluidic-based platforms have been examined for neuroscience applications.[35,36] An automated biomanufacturing approach which integrates the fabrication and biofunctionalization steps in an interwoven format could allow for enhanced design customization and improve the accuracy of the resultant model.

Here we describe a multiscale, 3D printed biomimetic system that reconstitutes the critical function of glial cell–axon

[a] *Department of Industrial and Systems Engineering, Virginia Tech, Blacksburg, Virginia 24061, USA*
[b] *Department of Mechanical and Aerospace Engineering, Princeton University, Princeton, New Jersey 08544, USA*
[c] *Department of Molecular Biology and Princeton Neuroscience Institute, Princeton University, Princeton, New Jersey 08544, USA*
[d] *Department of Mechanical Engineering, University of Minnesota, Minneapolis, Minnesota 55455, USA. E-mail: mcalpine@umn.edu*

† Electronic supplementary information (ESI) available: Micrographs of 3DNSC fabrication, viable cell printing, scanning electron micrograph characterization of 3D printed microchannels on protein-coated substrates, rapid prototyping of the 3DNSCs, comparison of viral transport imaging on different substrate materials, and association of Schwann cells and axons within microchannels. Supporting information is available online or from the author. See DOI: 10.1039/c5lc01270h

interfaces in the nervous system. Our bioinspired 3D printed device models various aspects of the complex and integrated organ-level responses to viral infections occurring within the nervous system. The device includes 3D printed topography[37] in the form of microchannels for axonal alignment and compartmented chambers for cell isolation. Viral infection studies suggest that Schwann cells participate in axon-to-cell spread *via* interactions with axonal pathways. We found that Schwann cells and hippocampal neurons were refractory to pseudorabies virus (PRV) infection transmitted from axons, suggesting a bottleneck to virus transmission. This work shows that 3D printing provides a valuable platform for the development of a customizable nervous system on a chip. Ultimately, 3D printed multiscale device architectures that reconstitute neural-tissue interfaces critical to organ function may expand the capabilities of cell culture models and provide viable alternatives to animal studies for fundamental research, drug screening, and toxicology applications.

Materials and methods

Harvesting and preparation of superior cervical ganglia and hippocampal neurons

Primary embryonic sensory neurons from the superior cervical ganglia (SCG) and hippocampal neurons were obtained from Sprague-Dawley rats (embryonic day 15.5–16.5, Hilltop Labs Incorporated, Pennsylvania, United States). For each study, the animal was euthanized and handled in strict accordance with good animal practice as defined by the relevant national and local animal welfare bodies, and approved by the Princeton University Institutional Animal Care and Use Committee (IACUC). SCGs were first harvested and then dissociated. For the isolation of hippocampal neurons, hippocampal tissue was harvested from the same embryos used to obtain SCG neurons. A detailed procedure can be found elsewhere.[38,39]

3D printing of the nervous system on a chip

Printer path information for the substrate microchannels and tri-chambers was constructed using vendor-provided software (Smart Robot, Fisnar) and computer-aided design (CAD) software (PTC Creo Parametric), respectively. CAD models were first converted to printer path information (G-code) using a cross-platform slicing program (KISSlicer), and subsequently converted to robot-specific language and transmitted to the robot using a custom LabVIEW program. 3D printing was done using a custom system consisting of a three-axis gantry industrial robot (F5200N, Fisnar, Wayne, NJ) with an external I/O card, a digital high precision dispenser (Ultimus V, Nordson EFD, Westlake, OH), and a fixed stage (ThorLabs). Silicone (RTV, Loctite), polycaprolactone (Sigma), and cell suspensions were printed using extruder tips which ranged from 27 to 32 gauge (GA). Stage levelling within 1 μm was achieved using a digital CMOS laser sensor (Keyence, Itasca, IL). Two types of 35 mm dishes were used, plastic dishes (CELLTREAT) and dishes which contained glass inserts (MatTek Corporation). Printing was conducted directly on poly-L-ornithine and laminin-coated petri dishes.

Functionalization and culturing of the 3DNSC

Following 3D printing, the three individual chambers were functionalized with hippocampal neurons, SCG neurons, Schwann cells (S16, CRL-2941, ATCC), and epithelial cells (porcine kidney 15, PK-15 cells) according to the following procedures. Neurons were the first cells added to establish a robust axonal network prior to adding the Schwann and epithelial cells. Two chip designs were examined: 1) peripheral nervous system (PNS) chip models, and 2) central nervous system (CNS) chip models. SCG neurons were added to chamber 1 for PNS chips and chamber 2 for CNS chips. Hippocampal neurons were added to chamber 1 for CNS chips (PNS chips contained no hippocampal neurons). Neuronal cultures were maintained at 37 °C and 5% CO_2 and by replacing half of the medium every 5–7 days with fresh growth medium. After the axonal network established by the primary neurons penetrated into each of the individual chambers, which took 10–14 days, Schwann cells and epithelial cells were added to the other compartments, which lacked neurons but contained robust axonal networks.

Fluorescence microscopy

Following cultivation of the mature chips, axons were stained for tau marker using anti-tau (monoclonal, mouse, Life Technologies), and epithelial cells were stained for cytokeratin marker using anti-cytokeratin (pan) (1 : 1000 in diluted blocking solution, polyclonal, rabbit, Life Technologies) and corresponding secondary antibodies (Alexa Flour 488 anti-mouse and Alexa Flour 568 anti-rabbit, Life Technologies). Imaging was carried out using a fluorescence microscope (Nikon Eclipse Ti, inverted epifluorescence microscope) as previously described.[40] Axon-associated Schwann cells were imaged *via* a three-colour coinfection system that utilized a mixture of three separate viruses each containing a different fluorophore expression cassette (mCeruelean, EYFP, or mCherry),[35] which provided enhanced resolution of axon-associated cell bodies.

Design and propagation of viral strains

All viral infection studies were conducted using pseudorabies virus (PRV). Epithelial cells were used to propagate and titre all PRV viral strains. PRV strains used in this study were previously constructed in our lab.[35] Strains for two types of infections were examined: three-colour infections and two-colour infections. For three-colour infections, the viruses used were constructed from three plasmids containing a CMV-modified immediate-early promoter, which drives the expression of a fluorescent protein fused to a tandem triplet repeat of a nuclear localization signal (NLS). A detailed explanation of the design, construction and validation is provided elsewhere.[41] Briefly, a EGFP-Us9 fusion gene was cloned into the gG locus of the PRV genome. This virus strain (designated PRV340)

was then co-infected at a multiplicity of infection (MOI) of 10 PFUs (plaque forming units) per cell with a mRFP-VP26 Us9-null strain (PRV325) previously generated in our lab.[42] We then isolated and purified individual fluorescent plaques expressing both GFP and mRFP *via* three rounds of consecutive plaque purification, resulting in the dual labelled virus designated PRV 341.

Quantification of viral transport

Mature SCG neurons were infected at a MOI of 10 PFUs per cell with the dual colour virus PRV341 (mRFP-VP26 and EGFP-Us9) and incubated for 8–12 h. Live imaging movies of the two-colour virus infections were acquired using near total internal reflectance fluorescence (TIRF) microscopy (also referred to as oblique angle microscopy) as previously described.[43] Briefly, virus particles were imaged on a Nikon Ti-E microscope in the Princeton University Molecular Biology Confocal Microscopy Facility. This microscope was equipped with 488 nm and 561 nm excitation lasers (Agilent), an Apo TIRF 100×/1.49 NA oil immersion objective (Nikon), an Andor iXon Ultra EMCCD camera, a 37 °C heated stage, and Nikon NIS Elements software. Fluorescence emission bands were as follows: EGFP, ~525/50 nm emission; mRFP, ~605/50 nm emission. The velocity of individual virus particles was calculated as the distance travelled per elapsed time.

Quantification of viral genome expression

Mature CNS chips were infected in chamber 2, which contained SCG neurons with an inoculum containing an equal mixture of each of the three viral strains containing a fluorescent cassette resulting in approximately 1×10^6 PFUs of a three-colour inoculum. Following 24 h of incubation, directly infected cells in chamber 2 as well as hippocampal neurons and Schwann cells in chambers 1 and 3, respectively, were imaged to estimate the average number of viral genomes expressed per cell following infection of SCG neurons with PRV at a high MOI as previously described.[44] Imaging was performed on a Nikon Ti-Eclipse inverted microscope equipped with separate fast-switching excitation and emission filter wheels (Prior Scientific) using a Plan Fluor 20× Ph objective (Nikon). For each experimental condition, at least two experiments were performed with three replicates.

Results and discussion

Design principle of the 3DNSC

The nervous system is composed of a complex network of neurons, neurites, glia, and ECM.[45] These components are organized into the CNS, consisting primarily of CNS neurons, astrocytes, and other supporting cells; and the PNS, consisting primarily of PNS neurons, axon-associated Schwann cells, and specialized axon termini that innervate peripheral tissues.[45] As shown in Fig. 1a, the inspiration for the 3DNSC is to provide a customizable, biomimetic *in vitro* model of the nervous system, with a one-to-one matching of the nervous system components within 3D printed platform chambers. Fabrication of the 3DNSC consisted of three steps, as outlined in Fig. 1b: 1) 3D printing of microchannels on a substrate to provide axonal guidance, 2) 3D printing of a

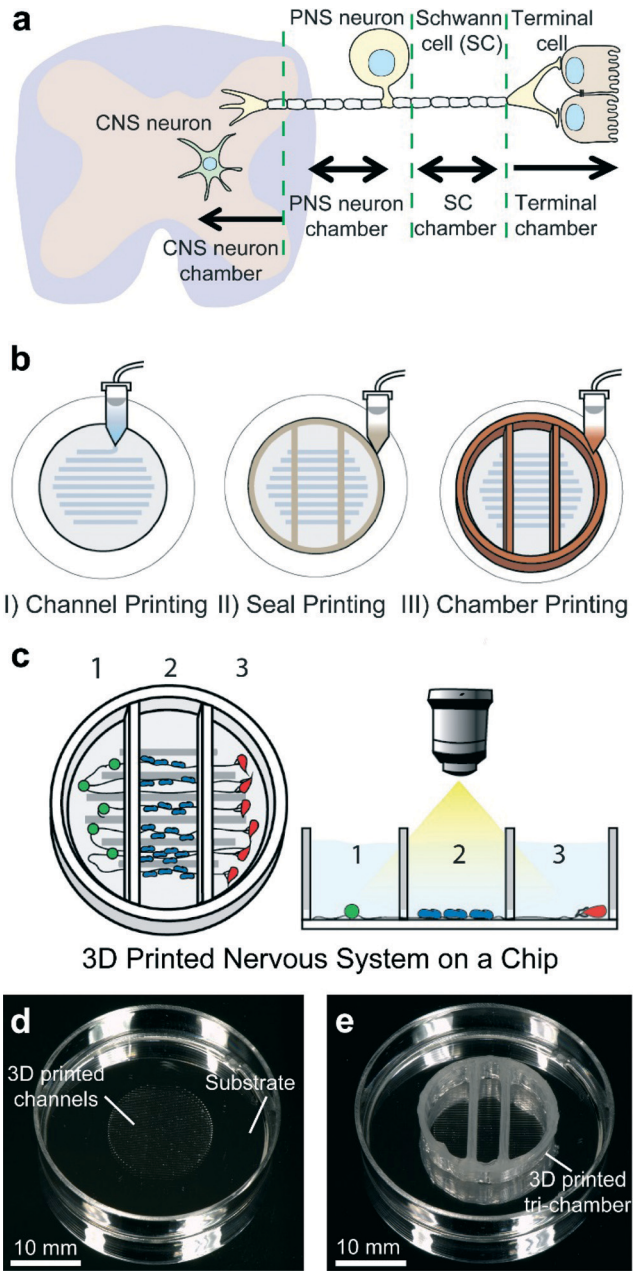

Fig. 1 a) Schematic of the nervous system, modelled as four primary components: CNS neurons, PNS neurons, axon-associated Schwann cells, and epithelial cells. b) 3D printing of the model nervous system on a chip, consisting of (I) parallel microchannels, (II) a sealant layer, and (III) a top tri-chamber. c) Schematic of a representative 3DNSC for peripheral nervous system applications, showing (1) PNS neurons in chamber 1, (2) Schwann cells in chamber 2, and (3) terminal cell junctions in chamber 3. The Schwann cells and the terminal cells interact with the neurons and each other solely *via* the axonal network. d) Circular pattern of 3D printed silicone microchannels for axonal guidance in the centre of a plastic 35 mm dish. e) A 3DNSC showing perpendicular assembly of microchannel and tri-chamber components.

substrate-chamber sealant layer to prevent fluid exchange among individual chambers, and 3) 3D printing of a top tri-chamber to provide isolation and organization of different cell types (*e.g.* neurons or glial cells). Following fabrication, the individual chambers were then functionalized with the desired cell types according to the mapping in Fig. 1a to achieve a mature 3DNSC (see Fig. 1c). One major advantage of this approach is the ability to readily establish separate fluid environments for neuronal axons and the soma from which they emanate. Thus, a perturbation to the nervous system – for example a viral inoculum – can be applied either to the compartment with the neuronal cell bodies, or to the compartment containing distal axons.

Fabrication of the 3DNSC

We initiated the manufacturing process by developing 3D computer models of both the substrate microchannels and the top tri-chamber, as shown schematically in Fig. 1b and c. As shown in Fig. 1d, the 350 μm wide 3D printed microchannels were constructed within a circular pattern (15 mm diameter) to optimize the percentage of cells on the chip which interact with axonal pathways. The width and inter-distance of the microchannels can be precisely tuned by controlling the dispensing time during the 3D printing process. As shown in Fig. 1e, the top tri-chamber was 18 mm in diameter and 10 mm high, and contained two inner walls, which resulted in three adjacent 6 mm wide chambers. Computer models of the 3DNSC microchannels and tri-chamber components are provided in Fig. S1 of the ESI.† The model for the sealant layer was identical to the top tri-chamber model, but the height was equal to that of a single layer (~150 μm). Both silicone and polycaprolactone were selected as the materials for direct microchannel printing onto protein-coated plastic dishes (printing time = 10 min; see Movie S1†). Following microchannel printing, the top tri-chamber and sealant layers were subsequently printed (printing time = 50 min; see Movie S2†). Silicone and grease served as the 3D printed materials for the tri-chamber and sealant layer, respectively. Thus, each 3DNSC required *ca.* one hour in total to fabricate. This throughput may be improved in the future *via* the use of multiplexed extrusion approaches, or by increasing the linear speed of the extruder, which was in the range of 0.1–1 mm s^{-1}. Assembly of the 3D printed substrate and top chamber components resulted in a complete 3DNSC. A distinguishing feature of the 3D printed *in vitro* systems relative to conventional compartmented chamber and microfluidic systems is the rapid prototyping capability, which we highlight in Fig. S2–S5.†

Functionalization and biomimetic maturation of the 3DNSC

We next functionalized the individual chambers of the chip with appropriate cell types. As a proof of concept, we also examined the functionalization of the chambers *via* direct 3D printing of cells (see Fig. S1†). As shown in Fig. 1a, the nervous system may be modelled as four primary interacting components which are connected by axons: 1) CNS neurons, 2) PNS neurons, 3) Schwann cells, and 4) epithelial cells. Thus, we examined two 3DNSC models with the tri-chamber (1–2–3) design: a peripheral 3DNSC consisting of PNS neurons-Schwann cells-epithelial cells, and a central 3DNSC consisting of CNS neurons-PNS neurons-Schwann cells. We first developed a peripheral 3DNSC. As shown in Fig. 2a, a peripheral 3DNSC was constructed which contained SCG neurons in chamber 1 (1), Schwann cells in chamber 2 (2), and PK-15 cells in chamber 3 (3). Fig. 2b–g show the alignment of the axons and the organization of cell types within the printed microchannels. Associated phase contrast micrographs can be found in Fig. S6.†

Several important conclusions can be drawn from Fig. 2b–g, which reveal effective biomimicry of the nervous system: 1) spatial separation of different cell types is achieved over micrometre to centimetre scales, 2) Schwann cells spontaneously associated with axons (see Fig. S7†), and 3) the axonal network penetrates into all chambers, providing the opportunity for axon-to-cell connections between the organized cells. Additional analysis of Schwann cell–axon association is provided in Fig. S7.† Given the complexity of the nervous system, there are many native physical (*e.g.* topographical, mechanical, and structural), biochemical, and cellular features which may ultimately be mimicked. Our proof-of-concept approach for demonstrating the application of 3D printing for *in vitro* model manufacturing involves the CNS–PNS junction. Therefore, focus here is placed on biomimicry of the cellular compartmentalization and topography, which establishes highly aligned axonal networks which contain associated Schwann cells.

In vitro model for physiologically relevant viral infection assays

Having shown that 3DNSCs exhibit biomimetic structures, we next focused on applying the chip to physiologically relevant organ-level viral infection studies. An understanding of viral infection and transport in the nervous system is critical to developing future treatments for various neurological diseases and disorders.[46,47] Therefore, we created 3DNSCs containing additional CNS components, *i.e.*, central 3DNSCs.

The central 3DNSC design is shown in Fig. 3a and consists of (1) CNS neurons (hippocampal neurons) in chamber 1, (2) PNS neurons (SCG neurons) in chamber 2, and (3) Schwann cells in chamber 3. As shown schematically in Fig. 3a, the viral assay involves infecting only chamber 2 – which contains the PNS neurons (SCGs) – with pseudorabies virus (PRV). We then monitored the axon-to-cell spread of viral particles to both hippocampal neurons (chamber 1) and Schwann cells (chamber 3).

As shown in Fig. 3b, we used a two-colour infection assay combined with oblique angle fluorescence microscopy to show that: 1) SCG neurons were infected by PRV, and 2) PRV was replicated by the SCG neurons, as indicated by the observation of immature (red capsid) and mature virus particles

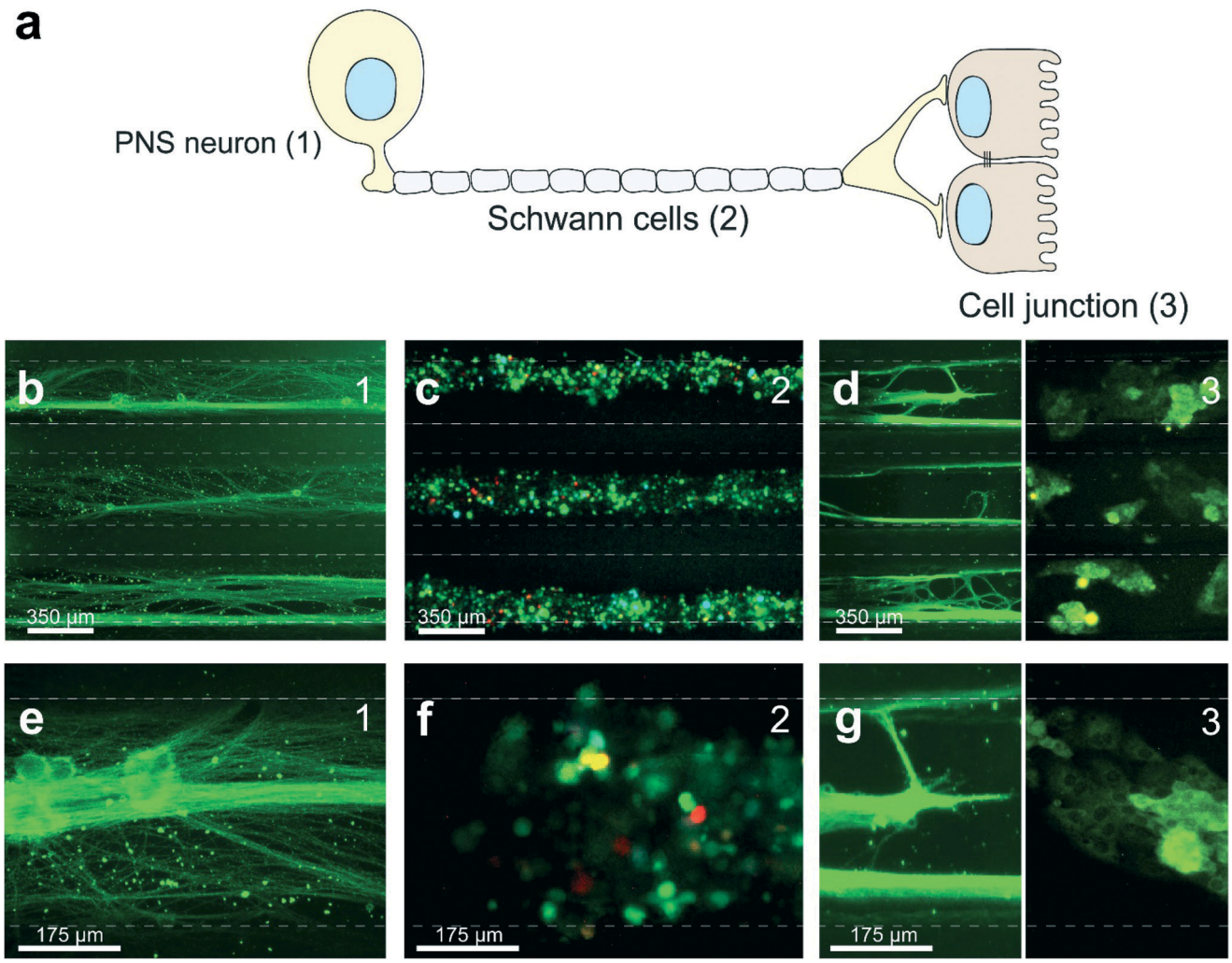

Fig. 2 a) Schematic of a peripheral 3DNSC showing three primary components: (1) the neuronal component and source of axons containing SCG neurons in chamber 1, (2) the peripheral nerve component containing axons and Schwann cells in chamber 2, and (3) the terminal cell junction component containing axon termini and epithelial cells in chamber 3. b) Micrograph showing three parallel microchannels of SCG neurons and axons (green tau stained) in chamber 1. c) Micrograph showing three parallel channels of peripheral nerve fibres containing organized self-assembled networks of axon-associated Schwann cells (tri-colour PRV Brainbow strain; see Materials and methods section) in chamber 2. d) Micrograph showing three parallel channels of axon termini (green tau stained) and epithelial cells (green cytokeratin stained) in chamber 3. e) Single channel image of neurons from (b). f) Single channel image of Schwann cells from (c). g) Single channel image of axon termini and epithelial cells from (d). Phase contrast images are provided in Fig. S6.†

(yellow puncta, a result of the red capsid tag co-localizing with the green envelope protein, suggesting a fully assembled particle) in the nucleus and axons. Rapid prototyping of chips on glass substrates also enabled calculation of the virus axonal transport rate as 2.0 μm s^{-1} *via* high-resolution imaging studies (Fig. S5†). The results shown in Fig. 3b suggest that SCG neurons are infected by PRV, and viral particles are transported within the axonal network of chamber 2 (the point of infection).

We next examined the spread of infectious particles to the other regions of the 3DNSC. We used a three-colour ("Brainbow") infection assay, which functions on the principle that if SCGs are co-infected with multiple viruses expressing primary colours and spread many infectious units to subsequent cells (*e.g.* hippocampal and Schwann cells), then one would expect those cells to also express multiple colours. Given the high number of progeny viruses produced from a single infected cell, we would expect multiple infection events in each cell connected to the cell replicating the virus. As shown by the representative images in Fig. 3c–f, direct infection of PNS neurons (SCGs) under high MOI indeed led to replication and spread of infection to the CNS neurons and Schwann cells. However, as indicated by the fluorescence signal, CNS neurons and Schwann cells exhibited only single primary colours, and not a multicolour profile, suggesting that there is a bottleneck to virus transmission from PNS axons to these cell types. This bottleneck to viral spread and infection has been previously observed in other cell types and suggests that there is a viral or cellular factor limiting infection of a single cell by multiple virons.[35,44,48,49]

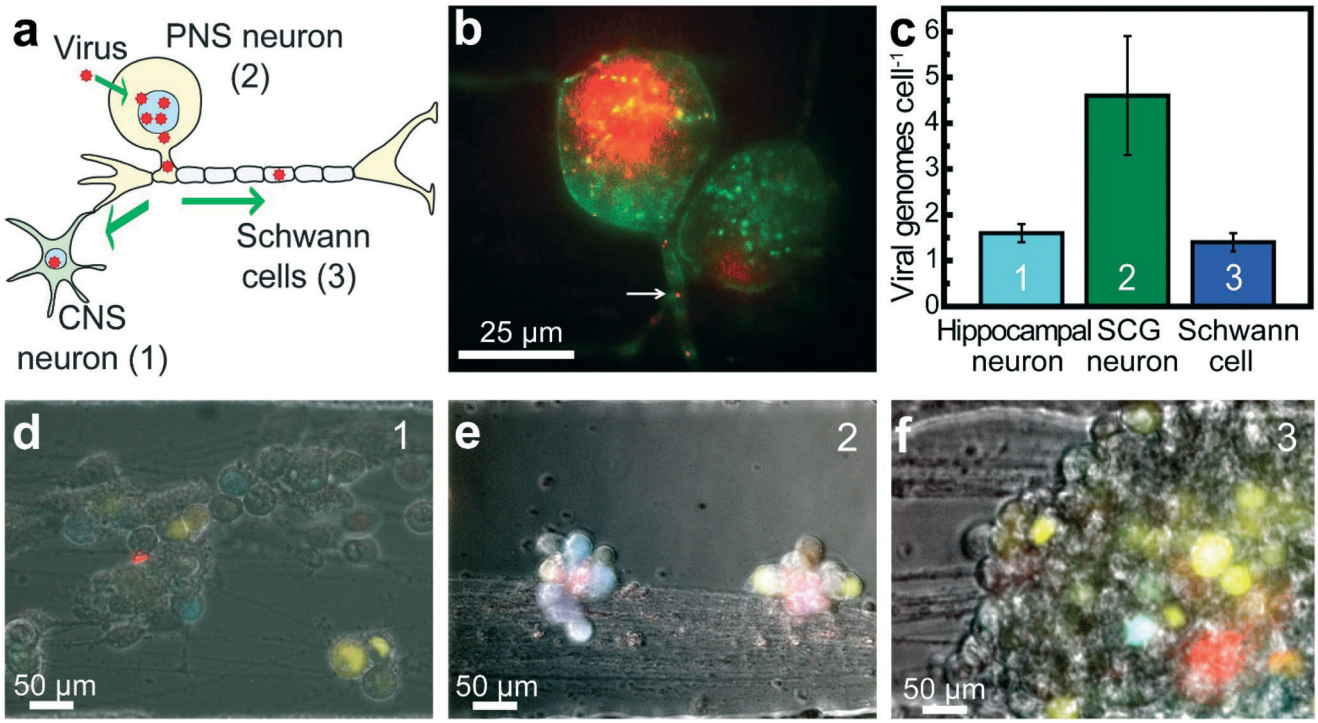

Fig. 3 a) Schematic of a central 3DNSC showing three primary components: (1) the CNS neuronal component containing hippocampal neurons in chamber 1, (2) the PNS neuronal component containing SCG neurons and sources of axons in chamber 2, and (3) the peripheral nerve component containing axons and Schwann cells in chamber 3. Arrows schematically depict the model viral infection assay, which involves infection of neurons in the PNS, and spread of the infection to the CNS neurons and Schwann cells. b) Total internal reflectance fluorescence (TIRF) micrograph of infected PNS neurons in chamber 2, with PRV two-colour viral strains showing replication and axonal transport of viral particles (arrow highlights a single virus particle). c) Estimated level of viral genome expression in infected cells found in chambers 1 and 3, originating from high MOI of PNS neurons in chamber 2. d) Micrograph of infected hippocampal neurons (1; PRV three-colour strains). e) Micrograph of infected SCG neurons (2; PRV three-colour strains). f) Micrograph of infected Schwann cells (3; PRV three-colour strains).

Given that the recombinant viruses are engineered to express primary colours when a single viral infection occurs, if more than one viral particle infects a cell, the colour profile will be altered, enabling one to estimate the number of virus genomes per cell *via* the following relation:[35,44]

$$\lambda = -3\ln\left(1 - \frac{r_1 + 2r_2 + 3r_3}{3n}\right) \quad (1)$$

where λ is the number of genomes expressed in each cell, r_1 is the number of one-colour cells, r_2 is the number of two-colour cells, r_3 is the number of three-colour cells, and n is the number of cells analysed. As shown in Fig. 3c, hippocampal neurons and Schwann cells showed similar restriction of viral uptake as indicated by 1.6 and 1.4 genomes per cell, respectively. This result reveals two new observations enabled by the 3DNSCs which are important for understanding infection mechanisms and barriers in the nervous system: 1) hippocampal neuron and Schwann cell types appear to be refractory to infection, and 2) Schwann cells appear to participate in infection response through axonal interaction. Importantly, the collective results in Fig. 3 demonstrate that 3DNSCs provide a flexible physiological platform for virology, molecular biology, and neuroscience assays which require the interrogation of system-level responses to localized perturbation (*e.g.* drugs, pathogens, electrical/mechanical energy, *etc.*).

Conclusions

In conclusion, 3D printing was used to create a nervous system on a chip by providing automated assembly of chambers and customized design of the microchannels and the chamber geometry. Viral assays were applied to demonstrate biological connectivity among the individual cellular components (*e.g.* neurons and glia), and to illustrate the flexibility and utility of the technology. Schwann cells and hippocampal neurons were found to be refractory to axon-to-cell infection of pseudorabies virus, suggesting a bottleneck to viral transmission. The successful integration of multiple neural components suggests that additive manufacturing may be used as an effective fabrication approach for the development of customizable organ-on-a-chip technologies. Future work will focus on: 1) direct patterning of neurons and glia, 2) extending this work to 3D microchannel networks,[50] 3) imaging of synapses and other close cell–cell contacts, 4) introducing CNS glial components, 5) examination of the neural electrical activity on physiological function, and 6) customization of CNS chips focused specifically on brain models.

Acknowledgements

We thank Dr. Paul Shao, Princeton Institute for the Science and Technology of Materials, and Department of Molecular Biology, for consultation and assistance with electron microscopy. B. N. J. and K. Z. L. contributed equally to this work. I. B. H. acknowledges the support of the American Cancer Society fellowship (PF-13-050-01-MPC). L. W. E. acknowledges the support of this work by the National Institutes of Health (NIH Grant No. R01NS033506 and Grant No. R01NS060699). M. C. M. acknowledges the support of the Defence Advanced Research Project Agency (DARPA Grant No. D12AP00245), and the Grand Challenges Program at Princeton University.

Notes and references

1 D. Huh, B. D. Matthews, A. Mammoto, M. Montoya-Zavala, H. Y. Hsin and D. E. Ingber, *Science*, 2010, **328**, 1662–1668.
2 D. J. Beebe, D. E. Ingber and J. den Toonder, *Lab Chip*, 2013, **13**, 3447–3448.
3 D. Huh, D. C. Leslie, B. D. Matthews, J. P. Fraser, S. Jurek, G. A. Hamilton, K. S. Thorneloe, M. A. McAlexander and D. E. Ingber, *Sci. Transl. Med.*, 2012, **4**, 159ra147.
4 A. D. van der Meer and A. van den Berg, *Integr. Biol.*, 2012, **4**, 461–470.
5 K. Yum, S. G. Hong, K. E. Healy and L. P. Lee, *Biotechnol. J.*, 2014, **9**, 16–27.
6 J. H. Sung, M. B. Esch, J.-M. Prot, C. J. Long, A. Smith, J. J. Hickman and M. L. Shuler, *Lab Chip*, 2013, **13**, 1201–1212.
7 L. Shintu, R. Baudoin, V. Navratil, J.-M. Prot, C. Pontoizeau, M. Defernez, B. J. Blaise, C. Domange, A. R. Péry, P. Toulhoat, C. Legallais, C. Brochot, E. Leclerc and M.-E. Dumas, *Anal. Chem.*, 2012, **84**, 1840–1848.
8 R. Booth and H. Kim, *Lab Chip*, 2012, **12**, 1784–1792.
9 P. Calvert, *Chem. Mater.*, 2001, **13**, 3299–3305.
10 V. Mironov, T. Boland, T. Trusk, G. Forgacs and R. R. Markwald, *Trends Biotechnol.*, 2003, **21**, 157–161.
11 A. Curodeau, E. Sachs and S. Caldarise, *J. Biomed. Mater. Res.*, 2000, **53**, 525–535.
12 S. Khalil, J. Nam and W. Sun, *Rapid Prototyp. J.*, 2005, **11**, 9–17.
13 E. Sachs, M. Cima, J. Cornie, D. Brancazio, J. Bredt, A. Curodeau, T. Fan, S. Khanuja, A. Lauder, J. Lee and S. Michaels, *CIRP Ann.*, 1993, **42**, 257–260.
14 B. Y. Ahn, E. B. Duoss, M. J. Motala, X. Guo, S.-I. Park, Y. Xiong, J. Yoon, R. G. Nuzzo, J. A. Rogers and J. A. Lewis, *Science*, 2009, **323**, 1590–1593.
15 A. Frutiger, J. T. Muth, D. M. Vogt, Y. Mengüç, A. Campo, A. D. Valentine, C. J. Walsh and J. A. Lewis, *Adv. Mater.*, 2015, **27**, 2440–2446.
16 Y. L. Kong, I. A. Tamargo, H. Kim, B. N. Johnson, M. K. Gupta, T.-W. Koh, H.-A. Chin, D. A. Steingart, B. P. Rand and M. C. McAlpine, *Nano Lett.*, 2014, **14**, 7017–7023.
17 J. W. Chang, S. A. Park, J.-K. Park, J. W. Choi, Y.-S. Kim, Y. S. Shin and C.-H. Kim, *Artif. Organs*, 2014, **38**, E95–E105.
18 B. Duan, L. A. Hockaday, K. H. Kang and J. T. Butcher, *J. Biomed. Mater. Res., Part A*, 2013, **101A**, 1255–1264.
19 L. A. Hockaday, K. H. Kang, N. W. Colangelo, P. Y. Cheung, B. Duan, E. Malone, J. Wu, L. N. Girardi, L. J. Bonassar, H. Lipson, C. C. Chu and J. T. Butcher, *Biofabrication*, 2012, **4**, 035005.
20 N. Herbert, D. Simpson, W. Spence and W. Ion, *J. Rehabil. Res. Dev.*, 2005, **42**, 141–146.
21 M. S. Mannoor, Z. Jiang, T. James, Y. L. Kong, K. A. Malatesta, W. O. Soboyejo, N. Verma, D. H. Gracias and M. C. McAlpine, *Nano Lett.*, 2013, **13**, 2634–2639.
22 S.-H. Ahn, K.-T. Lee, H.-J. Kim, R. Wu, J.-S. Kim and S.-H. Song, *Intl. J. Prec. Eng. Manuf.*, 2012, **13**, 631–634.
23 E. A. Roth, T. Xu, M. Das, C. Gregory, J. J. Hickman and T. Boland, *Biomaterials*, 2004, **25**, 3707–3715.
24 D. L. Cohen, E. Malone, H. Lipson and L. J. Bonassar, *Tissue Eng.*, 2006, **12**, 1325–1335.
25 A. Pfister, R. Landers, A. Laib, U. Hübner, R. Schmelzeisen and R. Mülhaupt, *J. Polym. Sci., Part A: Polym. Chem.*, 2004, **42**, 624–638.
26 S. V. Murphy and A. Atala, *Nat. Biotechnol.*, 2014, **32**, 773–785.
27 V. Mironov, N. Reis and B. Derby, *Tissue Eng.*, 2006, **12**, 631–634.
28 L. Krejcova, L. Nejdl, M. A. M. Rodrigo, M. Zurek, M. Matousek, D. Hynek, O. Zitka, P. Kopel, V. Adam and R. Kizek, *Biosens. Bioelectron.*, 2014, **54**, 421–427.
29 L. Gonzalez-Macia, A. Morrin, M. R. Smyth and A. J. Killard, *Analyst*, 2010, **135**, 845–867.
30 J. Rossiter, P. Walters and B. Stoimenov, *Proc. SPIE Electroactive Polymer Actuators and Devices*, 2009, vol. 7287, p. 72870H.
31 M. Matsusaki, K. Sakaue, K. Kadowaki and M. Akashi, *Adv. Healthcare Mater.*, 2013, **2**, 534–539.
32 J. B. Lee and J. H. Sung, *Biotechnol. J.*, 2013, **8**, 1258–1266.
33 I. Wagner, E.-M. Materne, S. Brincker, U. Sussbier, C. Fradrich, M. Busek, F. Sonntag, D. A. Sakharov, E. V. Trushkin, A. G. Tonevitsky, R. Lauster and U. Marx, *Lab Chip*, 2013, **13**, 3538–3547.
34 K. Schimek, M. Busek, S. Brincker, B. Groth, S. Hoffmann, R. Lauster, G. Lindner, A. Lorenz, U. Menzel, F. Sonntag, H. Walles, U. Marx and R. Horland, *Lab Chip*, 2013, **13**, 3588–3598.
35 M. P. Taylor, O. Kobiler and L. W. Enquist, *Proc. Natl. Acad. Sci. U. S. A.*, 2012, **109**, 17046–17051.
36 K. Sunja, P. Jaewon, H. Arum and L. Jianrong, *Neural Regener. Res.*, 2014, **9**, 1703–1705.
37 B. N. Johnson, K. Z. Lancaster, G. Zhen, J. He, M. K. Gupta, Y. L. Kong, E. A. Engel, K. D. Krick, A. Ju, F. Meng, L. W. Enquist, X. Jia and M. C. McAlpine, *Adv. Funct. Mater.*, 2015, **25**, 6205–6217.
38 D. Curanović, T. H. Ch'ng, M. Szpara and L. Enquist, in *Current Protocols in Cell Biology*, John Wiley & Sons, Inc., 2009, vol. 43, pp. 26.24.21–26.24.23.
39 T. H. Ch'ng and L. W. Enquist, *J. Virol.*, 2005, **79**, 10875–10889.
40 M. Taylor, R. Kratchmarov and L. Enquist, *J. Visualized Exp.*, 2013, 78, DOI: 10.3791/50723.

41 M. P. Taylor, T. Kramer, M. G. Lyman, R. Kratchmarov and L. W. Enquist, *mBio*, 2012, **3**, e00063.
42 M. G. Lyman, B. Feierbach, D. Curanovic, M. Bisher and L. W. Enquist, *J. Virol.*, 2007, **81**, 11363–11371.
43 I. B. Hogue, J. B. Bosse, J. R. Hu, S. Y. Thiberge and L. W. Enquist, *PLoS Pathog.*, 2014, **10**, e1004535.
44 O. Kobiler, Y. Lipman, K. Therkelsen, I. Daubechies and L. W. Enquist, *Nat. Commun.*, 2010, **1**, 146.
45 A. Brodal, *Neurological anatomy in relation to clinical medicine*, Oxford University Press, New York, USA, 1981.
46 L. E. Pomeranz, A. E. Reynolds and C. J. Hengartner, *Microbiol. Mol. Biol. Rev.*, 2005, **69**, 462–500.
47 J. R. Crawford, *Curr. Neurol. Neurosci. Rep.*, 2010, **10**, 147–154.
48 J. K. Pfeiffer and K. Kirkegaard, *Proc. Natl. Acad. Sci. U. S. A.*, 2006, **103**, 5520–5525.
49 K. Z. Lancaster and J. K. Pfeiffer, *PLoS Pathog.*, 2010, **6**, e1000791.
50 S. Pautot, C. Wyart and E. Y. Isacoff, *Nat. Methods*, 2008, **5**, 735–740.